Supporting Information for

A Microfluidic Impedance Cytometry Device for Robust Identification of *H. pluvialis*

Xiaoming Chen,[*a, b] Mo Shen,[a, b] Chungang Wu,[a, b] Zhipeng Song,[a, b] Jishun Shi,[a, b] Shun Liu,[a, b] and Yong Zhao*[a, b]

[a]*School of Control Engineering, Northeastern University at Qinhuangdao, Qinhuangdao 066004, PR China. E-mail: chenxiaoming@neuq.edu.cn*
[b]*Hebei Key Laboratory of Micro-Nano Precision Optical Sensing and Measurement Technology, Qinhuangdao, 066004, PR China. E-mail: zhaoyong@ise.neu.edu.cn.*

Section 1: Comparation with other microfluidic impedance cytometry systems for detection of microalgae

Table S1 Comparation with other microfluidic impedance cytometry systems for detection of microalgae

Reference	Electrode structure	Materials of electrodes	Wiring scheme	Experimental parameters	Throughput	Analysed sample
T. Tang. et al [1]	Planar electrode	Cr/Au electrodes	absolute	2.6 V 0.5 MHz and 6 MHz	900 cells/s	*Euglena*
T. Tang. et al [2]	Planar electrode	Cr/Au electrodes	differential	2.6 V 1 MHz	--	*Euglena*
T. Tang. et al [3]	Planar electrode	Cr/Au electrodes	differential	2.6 V 0.5 MHz and 6 MHz	1500 cells/s	*Euglena*
T. Tang. et al [4]	Planar electrode	Cr/Au electrodes	differential	1 V 0.5, 4, 7, 10 MHz	--	*Euglena*
J. Sui. et al [5]	Planar electrode	Au electrodes	absolute	1 V 0.5 MHz to 30MHz	--	*Picochlorum SE3*
G. Benazzi. et al [6]	Planar electrode	Ti:Au: Ti	differential	1 V 0.1, 1, 0.327 and 6.03 MHz	--	*Isochrysis galbana, Synechococcus sp. Rhodosorus m.*
D. S. de Bruijn .et al [7]	Planar eletrode	tantalum/platinum	absolute	0.5 MHz and 20 MHz	--	*Emiliania huxleyi*
Y. X. Song. et al [8]	3D electrode	Copper electrodes	absolute	1V 0.5 MHz and 3 MHz	--	*D. Salina*
X. Chen. et al [9]	Flat-end cylindrical electrode	Stainless steel wires	absolute	1V 0.5 MHz	1800 cells/s	*Euglena Oocystis sp*
This work	Flat-end cylindrical electrode	Stainless steel wires	absolute	1V 0.5 MHz, 1MHz, 3MHz and 5MHz	1800 cells/s	*Haematococcus pluvialis Euglena*

Section 2: Detailed derivation process

The complex impedance caused by capacitance effect of the cell mixture can then be calculated by[10, 11]

$$Z_C = \frac{4\pi k d_c}{j\omega\tilde{\varepsilon}_{mix} S} \tag{S1}$$

where k is the cell constant determined by the geometric parameters of the cells, d_c indicates the effective size of cells.

According to Maxwell's approximation, the conductivity of the mixture of fluid and cells is [12]

$$\sigma_{mix} = \sigma_m \left[1 + 2\varphi\left(\frac{\sigma_c - \sigma_m}{\sigma_c + 2\sigma_m}\right)\right] / \left[1 - \varphi\left(\frac{\sigma_c - \sigma_m}{\sigma_c + 2\sigma_m}\right)\right] \tag{S2}$$

$$\sigma_{mix} = \sigma_m \left[1 + 3\varphi \frac{\sigma_c - \sigma_m}{(1-\varphi)\sigma_c + (2+\varphi)\sigma_m}\right] \tag{S3}$$

The sensing region with the diameter D_d, and detection fluid and cells filled in the detection region. The resistance of the detection region with cells is

$$Z_R = \frac{4d}{\sigma_{mix}\pi D_d^2} \tag{S4}$$

The complex impedance $Z(\omega)$ of the detection region can be represented as follows[10]:

$$Z(\omega) = Z_C \cdot Z_R / (Z_C + Z_R) \tag{S5}$$

Based on the equation (S1), (S4) and (S5), impedances of the detection without and with cells are

$$Z_m = \frac{2kd_c d}{jfd\tilde{\varepsilon}_m S + kd_c\sigma_m\pi^2 D_d^2} \tag{S6}$$

$$Z_{mix} = \frac{2kd_c d}{jfd\varepsilon_{mix} S + kd_c\sigma_{mix}\pi^2 D_d^2} \tag{S7}$$

Therefore, the impedance change of the detection zone caused by cell is

$$\Delta Z = \frac{2kd_c d(jfd(\varepsilon_m - \varepsilon_{mix})S + kd_c(\sigma_m - \sigma_{mix})\pi^2 D_d^2)}{(jfd\varepsilon_m S + kd_c\sigma_m\pi^2 D_d^2)(jfd\varepsilon_{mix} S + kd_c\sigma_{mix}\pi^2 D_d^2)} \tag{S8}$$

Section 3: PDMS channel fabrication

Fabrication of channel mold with the dry films was carried out in a dark room environment without white light. Firstly, a dry film was applied onto a pristine glass surface submerged in water to ensure the removal of air bubbles trapped between them. Subsequently, an extruder was employed to expel the water from between the dry film and the glass. Afterward, we applied another layer of dry film onto the water surface using the same procedure as the first layer. Then, we covered dry films pasted on the glass with the pre-designed channel mask, and exposed it to ultraviolet light in the exposure box for 12 seconds. After removing the mask, dry film was put in a 1.5% Na2CO3 solution for 3 minutes to remove undesired structures. After further cleaning, the light-cured part of the dry film was retained to form a channel mold for subsequent processing of PDMS channel.

We mixed PDMS and curing agent at weight ratio of 10:1 and stirred for 120 seconds. Then, the mixture was poured onto the fabricated dry film channel mold, discharged the air bubbles in a vacuum box, and then heated in an oven at 80°C for 120 minutes to realize solidification of PDMS. We peeled off the microchannel, and drilled holes at the entrances and outlets to obtain the PDMS channel.

Section 4: Schematic diagram of experimental platform

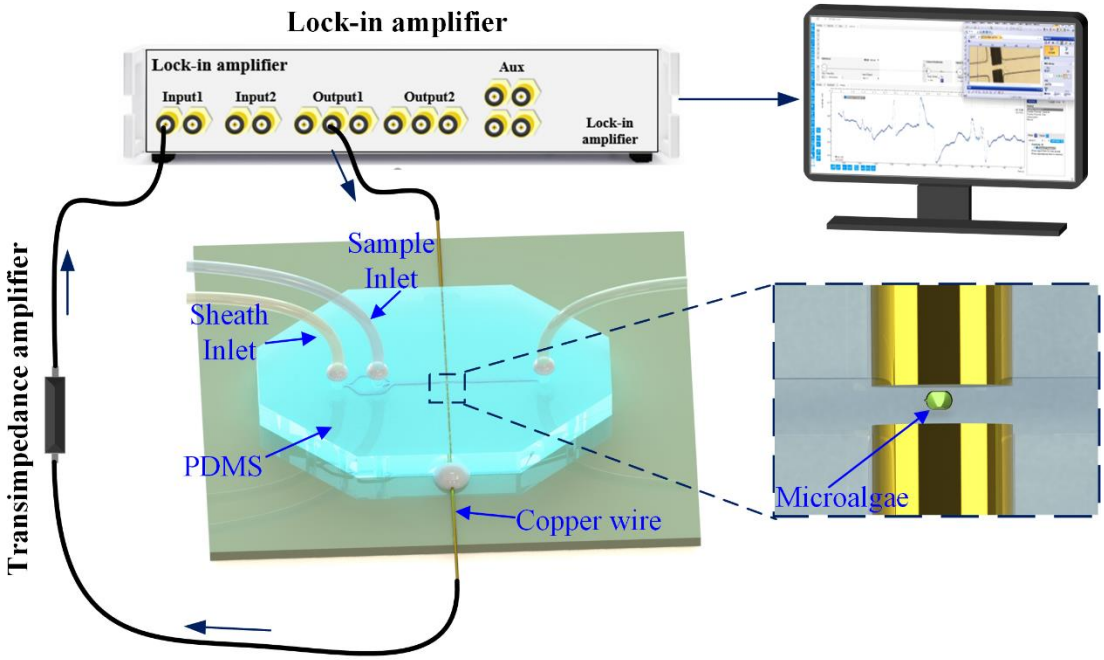

Figure.S1 Schematic diagram demonstrating the experimental system and wire connection.

Section 5: Calibration of polystyrene beads

All impedance signals are normalized based on the impedance signals of 20 µm beads and are denoted by the electrical diameter ($|Z|^{1/3}$)[13]. The electrical diameter of *H. pluvialis* cells can be calibrated based on that of 20 µm polystyrene beads. In theory, the impedance of polystyrene beads will not change with the change of frequency, and its electrical opacity should be 1. The polystyrene beads are detected at different frequencies with the simulation model, as shown in Figure.S2. Using single linear multipliers to ensure that the means of all impedance parameters of the beads are at opacity = 1 at each frequency.

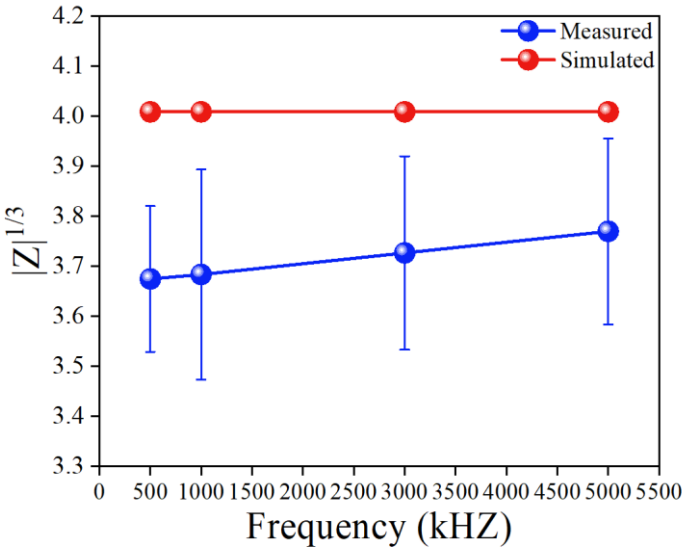

Figure.S2 Impedance of 20 µm polystyrene beads measured and simulated at different frequencies.

Section 6: Method of numerical simulation

We established the simulation model in the Comsol Multiphysics 6.0, and the flat-end cylindrical electrodes were equivalent to two circle surfaces on both sides of the fluid domain. The microalgae were equivalent to a sphere and ellipsoid. The module of Electric Currents was chosen to investigate the impedance change of microalgal cells in the detection process. In the simulation model, frequency domain was selected to study the impedance of the microalgal cells. After calculation, we input the equation of cell impedance and take the position of cell along X coordinate as sweep parameters. In this way, we can simulate the change of cell impedance in the dynamic detection. We also changed the distance between microalgae and detection zone center in the microchannel to simulate the travel process of microalgae in the detection. In this way, we can numerically investigate the impedance change of microalgae when they travel through the detection region. The following figure shows the conditions employed on and parameters of the simulation model.

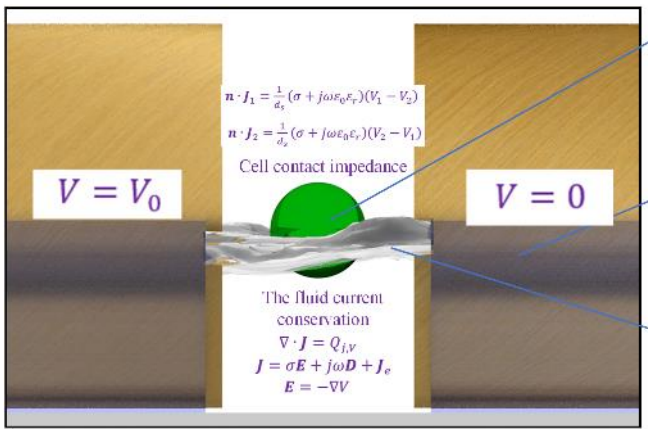

Cell

Relative permittivity of the cells	ε_c	60
Conductivity of the cells	σ_c	0.065
Density of the cells	ρ_c	1000 kg/m^3
Volume fraction of cells	φ	0~1
Cell constant	k	80~200
Radius of microalgae	R_c	10 μm

Channels and electrodes

Length of detection channel	L	400 μm
Width of detection channel	W	40 μm
Height of detection channel	H	81 μm
Radius of the flat-end electrode	R	40 μm

Solution

Conductivity of the solution	σ_m	0.2 S/m
Relative permittivity of the solution	ε_m	80
Density of the solution	ρ_m	1000 kg/m^3
Dynamic viscosity of the solution	μ	0.0000055

Figure.S3 The details and parameters of the simulation.

Section 7: Repeatability of the experiment

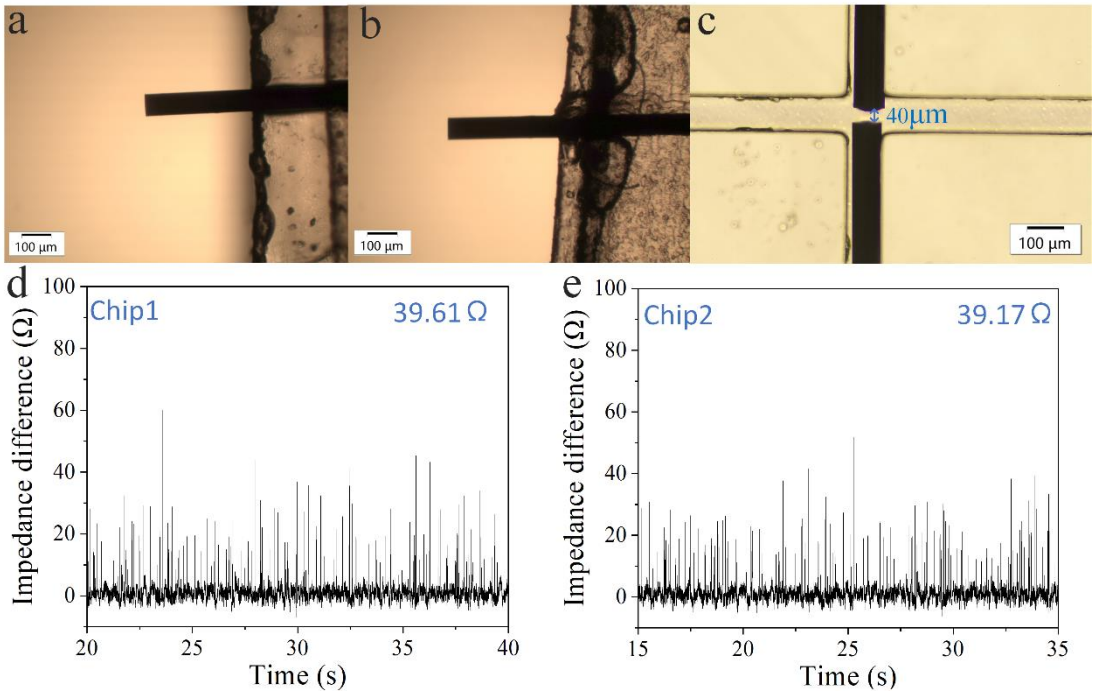

Figure.S4 Repeatability validation of the fabrication process. (a) Micrograph of the processed left electrode. (b) Micrograph of the processed right electrode. (c) Micrograph of the detection region after inserting and aligning the flat-end cylindrical electrodes in the wire channels. (d and e) Impedance of *H. pluvialis* cells detected with two microfluidic impedance cytometry with the electrode gap of 40 μm.

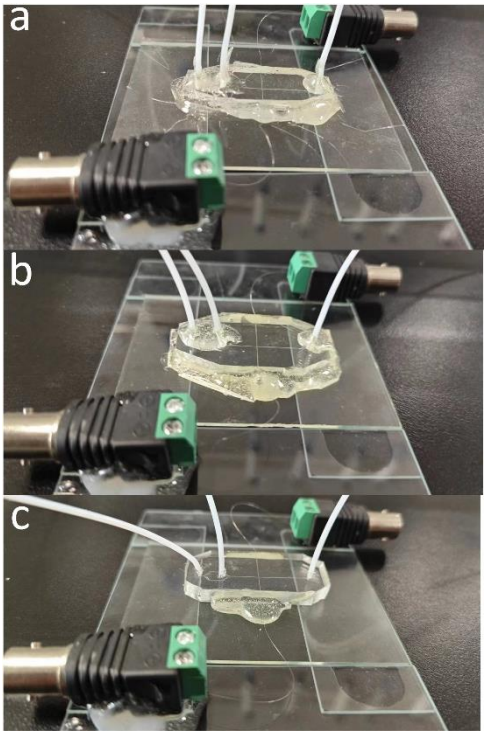

Figure.S5 Photograph of three microfluidic chips. (a) Chip 1. (b) Chip 2. (c) Chip 3.

Reference

1. T. Tang, X. Liu, Y. Yuan, R. Kiya, Y. Shen, T. Zhang, K. Suzuki, Y. Tanaka, M. Li, Y. Hosokawa and Y. Yalikun, *Lab on a chip*, 2022, **22**, 550-559.
2. T. Tang, X. Liu, R. Kiya, Y. Shen, Y. Yuan, T. Zhang, K. Suzuki, Y. Tanaka, M. Li, Y. Hosokawa and Y. Yalikun, *Biosensors and bioelectronics* 2021, **193**.
3. T. Tang, X. Liu, Y. Yuan, T. Zhang, R. Kiya, K. Suzuki, Y. Tanaka, M. Li, Y. Hosokawa and Y. Yalikun, *Sensors and actuators b: Chemical* 2022, **358**.
4. T. Tang, X. Liu, Y. Yuan, T. Zhang, R. Kiya, Y. Yang, K. Suzuki, Y. Tanaka, M. Li, Y. Hosokawa and Y. Yalikun, *Microsyst nanoeng* 2022, **8**, 68.
5. J. Sui, F. Foflonker, D. Bhattacharya and M. Javanmard, *Sci rep* 2020, **10**, 1251.
6. G. Benazzi, D. Holmes, T. Sun, M. C. Mowlem and H. Morgan, *IET nanobiotechnol*, 2007, **1**, 94-101.
7. D. S. de Bruijn, P. M. Ter Braak, D. B. Van de Waal, W. Olthuis and A. van den Berg, *Biosens bioelectron* 2020, **173**, 112808.
8. Y. X. Song, M. Q. Li, J. D. Yang, J. S. Wang, X. X. Pan, Y. Q. Sun and D. Q. Li, *Sensors and actuators b-chemical* 2014, **194**, 164-172.
9. X. Chen, M. Shen, S. Liu, C. Wu, L. Sun, Z. Song, J. Shi, Y. Yuan and Y. Zhao, *Lab on a Chip*, 2024.
10. Y. C. Xu, X. W. Xie, Y. Duan, L. Wang, Z. Cheng and J. Cheng, *Biosensors & bioelectronics* 2016, **77**, 824-836.
11. C. Petchakup, H. M. Tay, W. H. Yeap, R. Dalan, S. C. Wong, K. H. H. Li and H. W. Hou, *Biosensors & bioelectronics* 2018, **118**, 195-203.
12. T. Sun and H. Morgan, *Microfluidics and Nanofluidics*, 2010, **8**, 423-443.
13. D. C. Spencer, T. F. Paton, K. T. Mulroney, T. J. J. Inglis, J. M. Sutton and H. Morgan, *Nature Communications*, 2020, **11**.